Template banks to search for compact binaries with spinning components in gravitational wave data

Chris Van Den Broeck,[1,*] Duncan A. Brown,[2,†] Thomas Cokelaer,[1,‡] Ian Harry,[1,§] Gareth Jones,[1,‖] B. S. Sathyaprakash,[1,¶] Hideyuki Tagoshi,[3,**] and Hirotaka Takahashi[4,††]

[1]*School of Physics and Astronomy, Cardiff University, 5 The Parade, Cardiff, CF24 3YB, United Kingdom*
[2]*Department of Physics, Syracuse University, Syracuse, New York 13244, USA*
[3]*Department of Earth and Space Science, Graduate School of Science, Osaka University, Toyonaka 560-0043, Japan*
[4]*Department of Management and Information Systems Science, Nagaoka University of Technology, Nagaoka, Niigata 940-2188, Japan*

(Received 10 April 2009; published 10 July 2009)

Gravitational waves from coalescing compact binaries are one of the most promising sources for detectors such as LIGO, Virgo, and GEO600. If the components of the binary possess significant angular momentum (spin), as is likely to be the case if one component is a black hole, spin-induced precession of a binary's orbital plane causes modulation of the gravitational-wave amplitude and phase. If the templates used in a matched-filter search do not accurately model these effects then the sensitivity, and hence the detection rate, will be reduced. We investigate the ability of several search pipelines to detect gravitational waves from compact binaries with spin. We use the post-Newtonian approximation to model the inspiral phase of the signal and construct two new template banks using the phenomenological waveforms of Buonanno, Chen, and Vallisneri [A. Buonanno, Y. Chen, and M. Vallisneri, Phys. Rev. D **67**, 104025 (2003)]. We compare the performance of these template banks to that of banks constructed using the stationary phase approximation to the nonspinning post-Newtonian inspiral waveform currently used by LIGO and Virgo in the search for compact binary coalescence. We find that, at the same false alarm rate, a search pipeline using phenomenological templates is no more effective than a pipeline which uses nonspinning templates. We recommend the continued use of the nonspinning stationary phase template bank until the false alarm rate associated with templates which include spin effects can be substantially reduced.

DOI: 10.1103/PhysRevD.80.024009 PACS numbers: 04.30.Db, 04.25.Nx, 04.80.Nn, 95.55.Ym

I. INTRODUCTION

In 2005–2007, the Laser Interferometer Gravitational-Wave Observatory (LIGO) recorded two years of data at design sensitivity [1] and the LIGO, Virgo [2], and GEO600 [3] detectors now form a world-wide network of broadband gravitational-wave observatories. The LIGO and Virgo detectors are scheduled to resume operations in summer 2009 with a factor of ~2–3 sensitivity increase over previous observations. The gravitational waves emitted during the inspiral and merger of binaries containing neutron stars (NS) and/or black holes (BH) are a primary target of this network. Binary neutron stars (BNS) can be observed up to 35 Mpc (70 Mpc) in the Initial (Enhanced) LIGO detectors and up to 450 Mpc in the Advanced LIGO detectors, which will begin observations in 2015 [4]. Binary black holes (BBH) with $10M_\odot$ components should be visible at 170 Mpc (350 Mpc) in the Initial (Enhanced) LIGO detectors, increasing to 2 Gpc in Advanced LIGO [4]. Population synthesis calculations constrained by radio observations of BNS systems containing pulsars predict BNS detection rates between 10^{-3}–1 yr^{-1} for Enhanced LIGO and 0.4–400 yr^{-1} for Advanced LIGO, with the most likely values being 0.1 yr^{-1} and 40 yr^{-1}, respectively [4–6]. Much less is known about the detection rates of BBH and NS-BH coalescences, although it is plausible that Enhanced (Advanced) LIGO rates could be as high as 1(300) yr^{-1} for NS-BH binaries and 20(4000) yr^{-1} for BBH [4,7,8].

The sensitivities listed in the preceding paragraph are optimal: they assume accurate knowledge of the signal waveform in order to construct matched filters which can extract gravitational-wave signals buried in the noisy detector data [9,10]. The gravitational waveform from the inspiral of two compact objects has been calculated using the post-Newtonian (PN) approximation, which uses the characteristic velocity of the binary (v/c) as an expansion parameter [11–25]. Ongoing comparisons of PN waveforms with numerical simulations of binary black holes have thus far confirmed the accuracy of the PN solution in the late stages of inspiral [26–28], although optimal searches for sources with total mass $\gtrsim 30M_\odot$ in the first-generation detectors require waveforms that also model the merger and ringdown [29,30]. If the components of the

*Chris.van-den-Broeck@astro.cf.ac.uk
†dabrown@phys.syr.edu
‡Thomas.Cokelaer@astro.cf.ac.uk, Thomas.Cokelaer@inria.fr
§Ian.Harry@astro.cf.ac.uk
‖Gareth.Jones@astro.cf.ac.uk
¶B.Sathyaprakash@astro.cf.ac.uk
**tagoshi@vega.ess.sci.osaka-u.ac.jp
††hirotaka@oberon.nagaokaut.ac.jp

binary have negligible intrinsic angular momentum (spin) then it is straightforward to construct a *bank* of matched filters, parametrized by the two component masses of the binary, and use these filters to search for signals [31–34]. However, if the components of a binary are spinning, then these spins can couple with the orbital angular momentum of the binary and with each other to cause amplitude and phase modulation of the gravitational waveform [35]. Attempting to detect gravitational waves from spinning binaries with nonspinning templates will result in a suboptimal search and a corresponding reduction in the detection rate [36,37]. Since it is possible that a large fraction of astrophysical black holes have considerable spin [38,39], it is important to consider the effect of spin in searches for gravitational waves from BBH and NS-BH coalescences. However, optimal filters for spinning binaries are characterized by a much larger number of parameters than the ones for nonspinning binaries, complicating placement of filters in the bank and considerably increasing the computational cost of searches.

To mitigate the computational problem without compromising the sensitivity of the search, a phenomenological family of templates was proposed by Buonanno, Chen, and Vallisneri [40] (we refer to these templates as BCV spin). Filters constructed from these templates are described by only four parameters and have good overlaps with the full PN waveforms [40]. Moreover, constructing a bank of filters using BCV-spin waveforms is straightforward, if cumbersome [41,42]. The first searches for binary black hole signals in LIGO data used nonspinning templates [43,44], however BCV-spin templates were recently used to search for BBH and NS-BH signals with spin in data from the third LIGO science run [42]. The sensitivity of the search described in [42] was not as good as the main results of Ref. [40] might suggest. This was primarily due to the response of the BCV-spin template to the non-Gaussian noise transients present in real gravitational-wave detector data and the increase in the number of degrees of freedom associated with the detection statistic (due to the larger search parameter space) [42]. This was already anticipated in [40]; here we provide a quantitative analysis.

In this paper, we present an improvement to the search pipeline described in [42], by constructing banks that are much better suited to the BCV-spin template family. We compare the sensitivity of this search to the search for gravitational waves from compact binary coalescence with nonspinning templates in LIGO data [33,34]. Our main conclusion is that, while the BCV-spin templates have rather good overlaps with the target waveforms, the current search pipeline needs further improvements before any gains from these increased overlaps can be realized. The false alarm rate of BCV-spin filters in real detector data is larger than that of a nonspinning search. This makes a search using BCV-spin templates less sensitive than a nonspinning search when looking for binaries with spin, since one has to use a higher detection threshold to obtain the same false alarm rate. The results of this work were used to guide the decision *not* to implement the BCV-spin search on data from the fifth LIGO science run and instead to use nonspinning filters to search for binaries with spin [45]. The motivation for this decision was summarized in an appendix of Ref. [45] and this paper can be seen as a companion to that work. Here we present a detailed account of how the BCV-spin banks were constructed, and how the comparisons between the BCV spin and nonspinning searches were performed.

This paper is organized as follows. In Sec. II we give a description of our target signals, which are post-Newtonian waveform models for signals from spinning black hole binaries, followed by a summary, in Sec. III, of the phenomenological BCV-spin templates of Ref. [40]. In Sec. IV we review the construction of the template bank used in Ref. [42] and present two new methods to construct BCV-spin template banks, relaxing the assumptions used in Ref. [42]: a ''square-hexagonal'' placement which generalizes the hexagonal placement developed in [46] to a higher-dimensional template manifold, and a stochastic placement technique proposed in [47]. In Sec. V we compute matches of these banks with target waveforms and compare the results with those obtained from two-dimensional template banks based on the stationary phase approximation (SPA) [48,49] and hexagonal template placement used in LIGO's nonspinning searches [43–45,50–53]. We compare the detection efficiency of the spinning banks with that of SPA banks in Sec. VI followed by concluding remarks in Sec. VII. Throughout this paper, we set $G = c = 1$ unless otherwise stated.

II. POST-NEWTONIAN WAVEFORMS FROM SPINNING BINARIES

Depending on their birth spins, BH in binaries could accumulate significant spin through accretion [38,54]. There is much uncertainty concerning the equation of state of a neutron star, but most models place an upper limit $J/M^2 \lesssim 0.7$ on the spin, above which the star would break up [55]. There is also an upper limit for the spin of a black hole due to torque caused by radiation from the accretion disk getting swallowed by the BH, leading to an expected bound of $J/M^2 \lesssim 0.998$ [56]. Most of the modeling of spin evolution in compact binaries has been confined to NS-BH systems, in which case the spin tilt with respect to the orbital angular momentum can be considerable [38,54]; this may also be the case for BBH.

PN theory has achieved great success in modeling the adiabatic, quasicircular phase of inspiral, during which the fractional change in the orbital frequency over each orbital period will be negligible (see, e.g., Ref. [57] for a review). The orbital phasing has been calculated to order $(v/c)^7$ (or 3.5PN in the usual notation) [11–18,58–63] while the gravitational-wave amplitude for nonspinning binaries

has been calculated to order $(v/c)^6$ [13,19,20]. The effect of spin on the gravitational-wave phasing is known to order $(v/c)^5$, [21–24] and to order $(v/c)^3$ for the amplitude [25]. However, since the matched filter is most sensitive to the phase evolution of the binary, template waveform amplitudes are typically computed only at leading order in amplitude (the restricted waveform). Spin-orbit interaction enters the phasing at 1.5PN and 2PN order and spin-spin interaction at 2PN order. Spin effects influence the evolution of the orbital frequency as a function of time. Including these effects, the adiabatic evolution of the orbital frequency $\omega(t)$ is given by[1]

$$\frac{\dot{\omega}}{\omega^2} = \frac{96}{5}\eta(M\omega)^{5/3}\Bigg[1 - \frac{743+924\eta}{336}(M\omega)^{2/3} - \Bigg\{\sum_{i=1}^{2}\frac{\chi_i(\hat{\mathbf{L}}_N\cdot\hat{\mathbf{S}}_i)}{12}\Bigg(113\frac{m_i^2}{M^2}+75\eta\Bigg) - 4\pi\Bigg\}M\omega + \Bigg(\frac{34\,103}{18\,144} + \frac{13\,661}{2016}\eta + \frac{59}{18}\eta^2 - \frac{\eta\chi_1\chi_2}{48}[247(\hat{\mathbf{S}}_1\cdot\hat{\mathbf{S}}_2) - 721(\hat{\mathbf{L}}_N\cdot\hat{\mathbf{S}}_1)(\hat{\mathbf{L}}_N\cdot\hat{\mathbf{S}}_2)]\Bigg)(M\omega)^{4/3} - \frac{1}{672}(4159+15\,876\eta)\pi(M\omega)^{5/3} + \Bigg\{\Bigg(\frac{16\,447\,322\,263}{139\,708\,800} - \frac{1712}{105}\gamma + \frac{16}{3}\pi^2\Bigg) + \Bigg(-\frac{273\,811\,877}{1\,088\,640} + \frac{451}{48}\pi^2 - \frac{11\,831}{315}\Bigg)\eta + \frac{541}{896}\eta^2 - \frac{5605}{2592}\eta^3 - \frac{856}{105}\ln[16(M\omega)^{2/3}]\Bigg\}(M\omega)^2 + \Bigg(-\frac{4415}{4032} + \frac{717\,350}{12\,096}\eta + \frac{182\,990}{3024}\eta^2\Bigg)\pi(M\omega)^{7/3}\Bigg], \tag{1}$$

where $\hat{\mathbf{L}}_N$ is a unit vector in the direction of orbital angular momentum (and hence the unit normal to the orbital plane of the binary), $\mathbf{S}_{1,2}$ are the spins, $\chi_{1,2} = |\mathbf{S}_{1,2}|/m_{1,2}$ with $m_{1,2}$ the component masses, $\hat{\mathbf{S}}_{1,2} = \mathbf{S}_{1,2}/|\mathbf{S}_{1,2}|$, $M = m_1 + m_2$ is the total mass, and $\eta = m_1m_2/M^2$ the symmetric mass ratio. $\gamma = 0.577\ldots$ is the Euler-Mascheroni constant. The spins and the direction of the orbital angular momentum evolve according to [22,35]

$$\dot{\mathbf{S}}_1 = \frac{(M\omega)^2}{2M}\Bigg[\eta(M\omega)^{-1/3}\Bigg(4+3\frac{m_2}{m_1}\Bigg)\hat{\mathbf{L}}_N + \frac{1}{M^2}(\mathbf{S}_2 - 3(\mathbf{S}_2\cdot\hat{\mathbf{L}}_N))\hat{\mathbf{L}}_N\Bigg]\times\mathbf{S}_1, \tag{2}$$

$$\dot{\mathbf{S}}_2 = \frac{(M\omega)^2}{2M}\Bigg[\eta(M\omega)^{-1/3}\Bigg(4+3\frac{m_1}{m_2}\Bigg)\hat{\mathbf{L}}_N + \frac{1}{M^2}(\mathbf{S}_1 - 3(\mathbf{S}_1\cdot\hat{\mathbf{L}}_N))\hat{\mathbf{L}}_N\Bigg]\times\mathbf{S}_2, \tag{3}$$

$$\dot{\hat{\mathbf{L}}}_N = -\frac{(M\omega)^{1/3}}{\eta M^2}\dot{\mathbf{S}}, \tag{4}$$

where $\mathbf{S} = \mathbf{S}_1 + \mathbf{S}_2$. The dynamics of the binary is governed by the nonlinear, coupled differential equations (1)–(4). It will not be possible to solve these exactly, but they can easily be treated numerically.

By numerically evolving $\omega(t)$, one can obtain the orbital phase,

$$\Phi(t) = \int^t \omega\, dt, \tag{5}$$

which can be substituted into the usual expressions for the restricted PN waveform polarizations [64]. In the case of spinning binaries, we need to take into account the time dependence of the amplitudes through the inclination of the orbit with respect to the observer. The plus and cross polarizations of the gravitational wave are given by

$$h_+(t) = -[1 + (\hat{\mathbf{L}}\cdot\hat{\mathbf{n}})^2]\cos(2\Phi(t)),$$
$$h_\times(t) = -2(\hat{\mathbf{L}}\cdot\hat{\mathbf{n}})\sin(2\Phi(t)), \tag{6}$$

where the unit vector $\hat{\mathbf{n}}$ points from source to detector. The detector strain is

$$h(t) = F_+(t)h_+(t) + F_\times(t)h_\times(t), \tag{7}$$

where $F_{+,\times}(t) = F_{+,\times}(\alpha, \delta, \Psi(t))$ are detector antenna factors which depend on the right ascension and declination of the source and a time-dependent polarization angle $\Psi(t)$ (see, e.g., Ref. [35]).

As suggested by Eq. (4), the direction of orbital angular momentum and hence the plane of the inspiral will undergo precession, the effect being more pronounced for asymmetric systems. It will also be more prominent if the spins are large, and if they are significantly misaligned with the orbital angular momentum. The time evolution of spins and angular momentum will affect the phasing of the waveform through Eqs. (1)–(5), and the precession of the orbital plane will modulate the amplitudes of the wave polarizations in Eq. (6). The waveforms given by Eqs. (1)–(7) will be the ''target-signal waveforms'' for testing our template banks.

III. A DETECTION TEMPLATE FAMILY FOR SPINNING BLACK HOLE BINARIES

The frequency-domain phenomenological detection template family proposed in Ref. [40] is designed to capture spin-induced amplitude and frequency modulation in an approximate way. Specifically, for gravitational-wave frequencies $f > 0$, the BCV-spin template is

[1]At the time this work was started the spin-orbit term at 2.5PN [23,24] was not yet known and so is not included here.

$$\tilde{h}[t_0, \alpha_j'](f) = e^{2\pi i f t_0}\Theta(f_{\rm cut} - f) \times \left[\sum_{j=1}^{3}(\alpha_j' + i\alpha_{j+3}')h_j(f)\right]. \quad (8)$$

Here t_0 is the time of arrival, $\Theta(x)$ is the usual Heaviside step function, and $f_{\rm cut}$ is an upper cutoff frequency beyond which the waveform is unlikely to be close to a true signal (due to breakdown of the adiabatic approximation to the inspiral regime). The detection statistic will be maximized analytically over the parameters $\alpha_1', \ldots, \alpha_6'$ in the linear combination (8), as well as over t_0; these parameters are referred to as *extrinsic* parameters because they do not need to be explicitly searched over.

The waveforms $h_j(f)$, $j = 1, \ldots, 3$ are basis templates, which take the form

$$\tilde{h}_j(f) = \mathcal{A}_j(f)e^{i\Phi_{\rm NM}(f)}, \quad (9)$$

where

$$\mathcal{A}_1(f) = f^{-7/6}, \qquad \mathcal{A}_2(f) = f^{-7/6}\cos(\beta f^{-2/3}), \qquad \mathcal{A}_3(f) = f^{-7/6}\sin(\beta f^{-2/3}), \quad (10)$$

and β captures the effect of spin-induced amplitude modulation. The (nonmodulated) phase $\Phi_{\rm NM}(f)$ takes the form[2]

$$\Phi_{\rm NM}(f) = f^{-5/3}(\psi_0 + \psi_3 f). \quad (11)$$

It will not be possible to analytically maximize the detection statistic over the parameters ψ_0, ψ_3, and β, and these must be explicitly searched over using a bank of templates; they are referred to as *intrinsic* parameters.

It will often be useful to approximately identify the intrinsic parameters with the physical masses and spins of a compact binary. By relating ψ_0 and ψ_3 to the 0PN and 1.5PN phase coefficients [65], one has the correspondences

$$\psi_0 \leftrightarrow \frac{3}{128\eta}(\pi M)^{-5/3}, \qquad \psi_3 \leftrightarrow -\frac{3\pi}{8\eta}(\pi M)^{-2/3}. \quad (12)$$

Similarly, the parameter β can be related to the rate of precession by [35]

$$\beta \leftrightarrow 256\ {\rm Hz}^{2/3}\left(1 + \frac{3m_2}{4m_1}\right)\frac{m_1}{m_2}\left(\frac{M_\odot}{M}\right)^{2/3}\frac{|\mathbf{S}_1|}{m_1^2}. \quad (13)$$

We stress that these mappings are only approximate, and for a given physical signal, the detection template that matches best may correspond to values of (ψ_0, ψ_3, β) that differ significantly from the ones suggested by the identifications above.

The identifications (12) allow us to make a choice for $f_{\rm cut}$. In the limit where one component mass goes to zero while total mass M remains fixed, and assuming zero spins, the frequency of last stable orbit (LSO) of a test mass in the Schwarzschild spacetime is given by $f_{\rm LSO}(M) = (6^{3/2}\pi M)^{-1}$. For simplicity we set $f_{\rm cut} = f_{\rm LSO}(M)$, where $M = -\psi_3/(16\pi^2\psi_0)$ is computed from the correspondence (12).

Next, one constructs an orthonormal basis from the basis templates (9) with respect to the usual inner product for waveforms a, b on the template manifold given by

$$\langle a, b\rangle = 4\Re\int_{f_{\rm s}}^{f_{\rm cut}}\frac{\tilde{a}(f)\tilde{b}^*(f)}{S_n(f)}df, \quad (14)$$

where tilde denotes a quantity computed directly in the frequency domain (as in the case of the BCV-spin templates) or the Fourier transform of a time-domain quantity [such as the waveforms $h(t)$ given in Eq. (7)]. $S_n(f)$ is the one-sided power spectral density (PSD) of the detector data, and $f_{\rm s}$ is some lower cutoff frequency associated with the detector; in the case of initial LIGO one sets $f_{\rm s} = 40$ Hz. The orthonormalization of the basis templates can be effected using the Gram-Schmidt procedure as in [42]. In addition, one demands that the templates themselves are normalized (denoted by $\hat{h}$): $\langle\hat{h}, \hat{h}\rangle = 1$. This leads to the requirement

$$\sum_{j=1}^{6}\alpha_j^2 = 1, \quad (15)$$

where the α_j, $j = 1, \ldots, 6$, are the coefficients of $\hat{h}$ when expressed into the orthonormal basis of templates resulting from the Gram-Schmidt procedure.

Finally, the signal-to-noise ratio (SNR), which is used as the BCV-spin detection statistic, is given by

$$\rho = [\max_{t_0, \alpha_j}\langle s, \hat{h}[t_0, \alpha_j]\rangle]^{1/2}, \quad (16)$$

where s represents the detector data stream, and the maximization over the α_j is subject to the constraint (15).

IV. TEMPLATE BANKS FOR SPINNING BINARIES

The template waveforms h may not exactly model gravitational-wave signals s. The loss in SNR due to differences between the template and signal waveforms is quantified by the *fitting factor* $\mathcal{F}$ [35]. If s is a signal waveform and h a template waveform, then

$$\mathcal{F} \equiv \max_{\hat{h}}\langle\hat{s}, \hat{h}\rangle, \quad (17)$$

where the hat denotes normalization: $\langle\hat{s}, \hat{s}\rangle = \langle\hat{h}, \hat{h}\rangle = 1$. $1 - \mathcal{F}$ is the fractional loss in SNR resulting from the use of suboptimal template waveforms rather than the true signal waveforms. Since we do not *a priori* know the intrinsic parameters of any gravitational-wave signals we may detect, we decide on a target-signal space and construct a discrete bank of templates to search for signals in this space. If $\hat{h}_b$ is a normalized template waveform in the

[2]What is called ψ_3 here was denoted $\psi_{(3/2)}$ in [40].

discrete bank and $\hat{h}$ is a normalized waveform from the space used to construct the bank, then the minimum match $\mathcal{M}$ of the bank is defined to be [31]

$$\mathcal{M} \equiv \min_{\hat{h}} \left(\max_{\hat{h}_b \in \text{bank}} \langle \hat{h}, \hat{h}_b \rangle \right). \tag{18}$$

A typical choice for the minimum match in gravitational-wave searches is $\mathcal{M} = 0.97$. When measuring the performance of a template bank, we are interested in the *effective fitting factor* $\bar{\mathcal{F}}$ given by [66]

$$\bar{\mathcal{F}} = \max_{\hat{h}_b \in \text{bank}} \langle \hat{s}, \hat{h}_b \rangle. \tag{19}$$

If the signal waveforms are identical to those used to construct the bank, then the effective fitting factor will be bounded below by the minimum match. In practice, the true gravitational-wave signals will differ from the templates used to construct the bank, so the effective fitting factor may be smaller than the minimum match. The larger the effective fitting factor, the better the bank is at capturing the target signals.

If the parameters $\vec{\lambda}$ between two (normalized) templates differ by a small amount $\Delta\vec{\lambda}$, the loss in SNR can be related to a distance defined by a metric g_{ij} given by

$$\langle \hat{h}(\vec{\lambda}), \hat{h}(\vec{\lambda} + \Delta\vec{\lambda}) \rangle \simeq 1 - g_{ij} \Delta\lambda^i \Delta\lambda^j, \tag{20}$$

where

$$g_{ij} = \frac{1}{2} \left\langle \frac{\partial \hat{h}}{\partial \lambda^i}, \frac{\partial \hat{h}}{\partial \lambda^j} \right\rangle. \tag{21}$$

The standard method of constructing a template bank then consists of computing this metric in the intrinsic parameter space of a waveform family and using it to place templates such that the distance between any template waveform and the nearest template in the bank is greater than the desired minimum match $\mathcal{M}$. In searches for nonspinning binaries, the intrinsic parameters of the templates are the just component masses (m_1, m_2) of the binary. In practice, we reparametrize the waveforms using the chirp times $(\tau_0(m_1, m_2), \tau_3(m_1, m_2))$ [32]. With respect to these variables the metric is almost Euclidean, and so template placement using the metric g_{ij} becomes a straightforward two-dimensional hexagonal packing problem [33].

As described in Sec. I, a search for gravitational waves using the BCV-spin templates has been performed in S3 LIGO data [42]. The metric used in that analysis was computed using the "strong modulation approximation" where one assumes that the binary precesses many times while emitting in the most sensitive part of the detector's band. This allows one to treat the basis templates of Eq. (9) as orthonormal, simplifying the calculation of the metric. However, the resulting template banks were only appropriate for fairly low-mass, asymmetric systems. We now present an improved algorithm for constructing a metric in which the assumptions of [42] are dropped. In our case, the parameters of the waveform are

$$\vec{\lambda} = (t_0, \alpha_1, \ldots, \alpha_6, \psi_0, \psi_3, \beta). \tag{22}$$

The detection statistic can be maximized over the extrinsic parameters t_0 and $\alpha_1, \ldots, \alpha_6$, which, as shown in [67], leads to a projected metric g_{ij}^{proj} which only measures distances in the (ψ_0, ψ_3, β) directions. However, the *components* of g_{ij}^{proj} will still depend on the α_j. This residual dependence on extrinsic parameters can be removed as follows:

(1) Introduce some fiducial distance Δs_0.
(2) Specify a large number of unit vectors (in the coordinate sense) $\hat{n}$ in (ψ_0, ψ_3, β) space.
(3) For each $\hat{n}$, numerically maximize the *metric* length $\Delta s_{\hat{n}}$ computed from g_{ij}^{proj}, over values of the α_j consistent with the constraint (15); i.e.,

$$\Delta s_{\hat{n}}^2 = \max_{\sum_k \alpha_k^2 = 1} g_{ij}^{\text{proj}}(\alpha_m, \beta) \hat{n}^i \hat{n}^j. \tag{23}$$

(4) Rescale each vector $\hat{n}$ by defining a new vector $\bar{u} = (\Delta s_0 / \Delta s_{\hat{n}}) \hat{n}$.
(5) Fit an ellipsoid in parameter space to the vectors $\bar{u}$.
(6) Define an "effective" metric g_{ij}^{eff} by requiring that any point on the ellipsoid is at effective metric distance Δs_0 from the template we started with.

Note that this construction is independent of the fiducial length scale Δs_0. In what follows, g_{ij}^{eff} is the metric we will use to satisfy the criterion (18) through the relationship (20). A property of g_{ij}^{eff} is that it is essentially independent of ψ_0 and ψ_3 and only has a weak dependence on β.

It is important to note that, given a short straight line segment in coordinate space with coordinate length $\Delta\vec{\lambda}$, by construction g_{ij}^{eff} associates almost the largest possible metric length to it consistent with the family of metrics $g_{ij}^{\text{proj}}(\alpha_j, \beta)$ parametrized by the α_j. When generating template banks, in practice one specifies a minimum match which will then be used together with the metric to determine the spacing of templates. Since g_{ij}^{eff} is too conservative in assigning lengths, neighboring templates will tend to have a larger match than needed, and the true minimum match defined by (18) will always be significantly larger than what was originally intended. As we shall see below, setting an *a priori* value of $\mathcal{M} = 0.8$ will be more than enough for a bank to obtain high overlaps ($\gtrsim 0.9$) with target waveforms.

We would like to capture signals from binaries whose component masses are in the interval $[1, 35] M_\odot$, with total masses $M \leq 35 M_\odot$. We do not need to worry about capturing BNS signals, since spin does not have a significant effect on waveforms from those sources. However, our template bank should have good overlap with NS-BH

and BBH signals. Taking neutron star masses to lie between $1M_\odot$ and $3M_\odot$ and black hole masses to be larger than $3M_\odot$, we impose $M \geq 4M_\odot$. To capture these signals, we want an appropriately chosen bounding box in (ψ_0, ψ_3, β) within which to place templates. Such a box can be specified using the correspondences (12) and (13). The suggested intervals for (ψ_0, ψ_3) are then roughly

$$\begin{aligned} \psi_0 &\in [8 \times 10^3, 5 \times 10^5]\ \mathrm{Hz}^{5/3}, \\ \psi_3 &\in [-3 \times 10^3, 10]\ \mathrm{Hz}^{2/3}, \end{aligned} \tag{24}$$

where the upper bound for ψ_3 has been chosen generously. As to β, the correspondence (13) suggests that $\beta \lesssim 150\ \mathrm{Hz}^{2/3}$ should suffice, but to have good matches with a variety of physical signals, here too it turned out to be better to have a larger upper bound:

$$\beta \in [1, 4 \times 10^2]\ \mathrm{Hz}^{2/3}. \tag{25}$$

We now present two methods for constructing template banks for BCV-spin templates which cover this space.

A. Square-hexagonal template bank

The metric g_{ij}^{eff} depends only on β, so it is natural to first define layers of constant β, with a spacing determined by the minimum match. Within each of the two-dimensional layers, one can then lay out templates in a hexagonal pattern, which is the optimal placement in two dimensions. We will refer to this kind of placement as *square hexagonal*. The construction of this bank is analogous to that described in Ref. [46] which was used to construct template banks for search for binary black holes in data from the third and fourth LIGO science runs [44] using nonspinning phenomenological templates [68]. For the BCV-spin templates, we have a 3-metric, which in each β layer is diagonalized by going to a new set of coordinates $(\psi_0', \psi_3', \beta')$, where $\beta' = \beta$. After that a hexagonal placement in (ψ_0', ψ_3') can be performed as in [46]. As explained above, the metric is overly conservative in specifying distances between templates, and setting an *a priori* minimum match of $\mathcal{M} = 0.8$ will suffice to obtain high matches with target waveforms.

At this point we note that optimal coverings are known for high dimensions and have been studied in the context of other gravitational-wave searches by Prix [69]. For future higher-dimensional template banks that treat spin in a more comprehensive way than BCV spin does, a more optimal template placement may be in order. However, for BCV spin the number of templates will not be so high that the efficiency of our search will be compromised by the adoption of a more simple placement.

B. Stochastic template bank

We now consider a different bank placement for BCV spin, which we hope will reduce the overcoverage of the parameter space that is unavoidable with the square-hexagonal placement method defined above. This will lead to a smaller number of templates but will yield the same or better matches with target waveforms, and similar efficiencies. This template bank is created by the placement of a large number of randomly distributed templates, followed by a "pruning" stage in which unnecessary templates are discarded. This method is described in [47] and summarized below. Other, similar methods for creating stochastic template banks were proposed in [70,71].

The stochastic placement algorithm we wish to use for BCV spin is very simple. We begin by generating a very large number of points in the parameter space, far more than would be needed to fill the space. We then iteratively cycle through these points, retaining a point only if it is not closer than some predefined metric distance Δ to the points retained in previous iterations. The remaining points form our stochastically generated bank. Tests have shown [47] that one should begin with at least $N^{1.5}$ points, where N would be the number of templates remaining after filtering, to have a good coverage of the parameter space after pruning.

In testing this algorithm against lattice placement algorithms, it was found [47] that in a two-dimensional Cartesian space the stochastic algorithm produced a template bank with 1.5 times the number of templates that a square lattice algorithm would have generated. However, in the case of a two-dimensional nonspinning (non-Cartesian) SPA bank (as described above) the stochastic algorithm was found to place $\sim$10% less templates than the square lattice algorithm and only $\sim$25% more templates than the hexagonal lattice placement, while achieving a similar degree of coverage. We emphasize here that this stochastic placement algorithm would be of most use in parameter spaces with more than two dimensions, where lattice placement becomes significantly subobtimal.

For the specific case of BCV spin, the templates are sprinkled randomly over a rectangular box in (ψ_0, ψ_3, β) space using the same bounding box as in the previous subsection. An estimate for the number of templates that will be needed is provided by the invariant volume of the box, divided by the volume taken up by an individual template:

$$\mathcal{N} = \frac{\int_{\mathrm{box}} \sqrt{\det(g_{ij}^{\mathrm{eff}})}\, d\psi_0\, d\psi_3\, d\beta}{(1 - \mathcal{M})^{3/2}}. \tag{26}$$

Once again it will suffice to set an *a priori* minimum match $\mathcal{M} = 0.8$ (i.e., setting the Δ defined above to 0.2). Given the box in parameter space specified by (24) and (25), the number of sprinkled templates should then be about 500 000. When using a larger number of initial templates, we find that the final number of templates after pruning does not change significantly. With the Initial LIGO design PSD, the number of templates for stochastic BCV-spin banks with $\mathcal{M} = 0.8$ is about 8000; SPA banks with $\mathcal{M} = 0.95$ have $\sim$12 000 templates, and for BCV

TABLE I. Number of templates for the SPA, square-hexagonal, and BCV-spin banks with Initial LIGO design PSD, and median and mean effective fitting factors $\bar{\mathcal{F}}$ of the banks with target waveforms as in Fig. 1

Template	Bank placement	SNR threshold	Minimum match $\mathcal{M}$	Number of templates	$\bar{\mathcal{F}}_{\text{median}}$	$\bar{\mathcal{F}}_{\text{mean}}$
SPA	SPA	5.5	0.95	11 832	0.89	0.86
BCV spin	Square hexagonal	8	0.8	16 431	0.96	0.92
BCV spin	Stochastic	8	0.8	7913	0.96	0.93

spin with square-hexagonal placement and $\mathcal{M} = 0.8$ more than 16 000 templates are obtained (see Table I).

V. COMPARISON OF BCV-SPIN BANKS WITH SPINNING PN SIGNALS

We now study the performance of our banks against the target waveforms of Sec. II. In particular, for a variety of target waveforms s corresponding to different masses and initial spins, we compute the effective fitting factor $\bar{\mathcal{F}}$ of the bank for the target waveforms, as given by Eq. (19).

Figure 1 compares the effective fitting factor of templates in square-hexagonal and stochastic BCV-spin banks with those of a nonspinning SPA bank. There is no discernible difference between square-hexagonal and stochastic placements, but both differ significantly from the nonspinning SPA bank. As one would expect, the difference is largest for binaries with large mass ratios, although there is improvement also for a variety of other target waveform masses. Depending on masses and spins, for the same target waveform s, the difference in $\bar{\mathcal{F}}$ can be more than 25%. The medians and means for the effective fitting factors are summarized in Table I. We find that BCV-spin with stochastic bank placement has marginally better effective fitting factors than the square-hexagonal bank, and both BCV-spin banks have noticably higher effective fitting factors than the nonspinning bank. Given the small difference between the stochastic and square-hexagonal BCV-spin banks we will subsequently only consider differences between the stochastic BCV-spin bank and the nonspinning SPA bank.

VI. SEARCH PERFORMANCE OF BCV-SPIN TEMPLATE BANKS

The effective fitting factor of a target waveform over a template bank as defined in Eq. (19) indicates how similar the templates are to physical signals, but when searching for gravitational-wave signals in real detector data, other factors also come into play. The effective fitting factor of a template bank gives us a measure of how the signal-to-noise ratio is reduced by not filtering with the true signal waveform, but to detect a signal we must be able to distinguish it from background noise in the detector. To determine the overall performance of a template bank, we have to consider both the effective fitting factor and the *false alarm rate* of the bank, i.e., the response of the filters to noise (both Gaussian and transient) in the detector. Once we establish the false alarm rate of a search, we measure the performance of a bank by its *efficiency*, i.e., the bank's ability to find simulated target waveforms injected in the noise at a given false alarm rate. We will establish the false alarm rates and efficiencies of BCV spin and SPA banks by means of the data-analysis pipeline used in searches by the LIGO Scientific Collaboration (LSC) for inspiral signals [42,44,45], which is available in the LSC Algorithm Library [72]. More details on this pipeline can be found in Ref. [73].

A. False alarm rates

The BCV-spin detection statistic (16) involves maximization over six parameters (t_0, and the α_j with the constraint $\sum_j \alpha_j^2 = 1$), to be compared with only two for SPA. It should also be noted that the BCV-spin detection template family consists of waveforms that are only approximate. As we shall see below, the larger number of degrees of freedom will make the BCV-spin banks more prone to detecting instrumental noise transients with high SNR. Both for SPA and BCV spin, one needs to set an SNR threshold below which no candidate events are accepted, and the higher false alarm rate with BCV spin will necessitate setting a higher threshold.

The pipeline used to search for gravitational-wave signals in the LIGO detectors demands that candidate events be coincident in two or more detectors [73]. If the noise sources in our detectors are uncorrelated (as in the case of the two 4 km LIGO detectors), we can measure the false alarm (or background) rate of this pipeline by time shifting the detector data by more than the gravitational-wave travel time between the detectors (11 ms) and looking for coincident triggers; such triggers will be due to accidental coincidence of noise alone. We can repeat this with time steps of, say, 10 s, and count the number of coincident triggers in each of the time shifts to obtain a good estimate of the false alarm rate.

Before triggers are compared between detectors, they are clustered together, keeping only the trigger with the loudest SNR within a certain time window (in our case 400 ms). Next, various methods can be used for declaring two clustered triggers to be coincident across detectors. Usually one demands not only coincidence in time, but also that the parameters of the template that gave the loudest SNR be similar in the different detectors. The simplest way of implementing this is the so-called box-

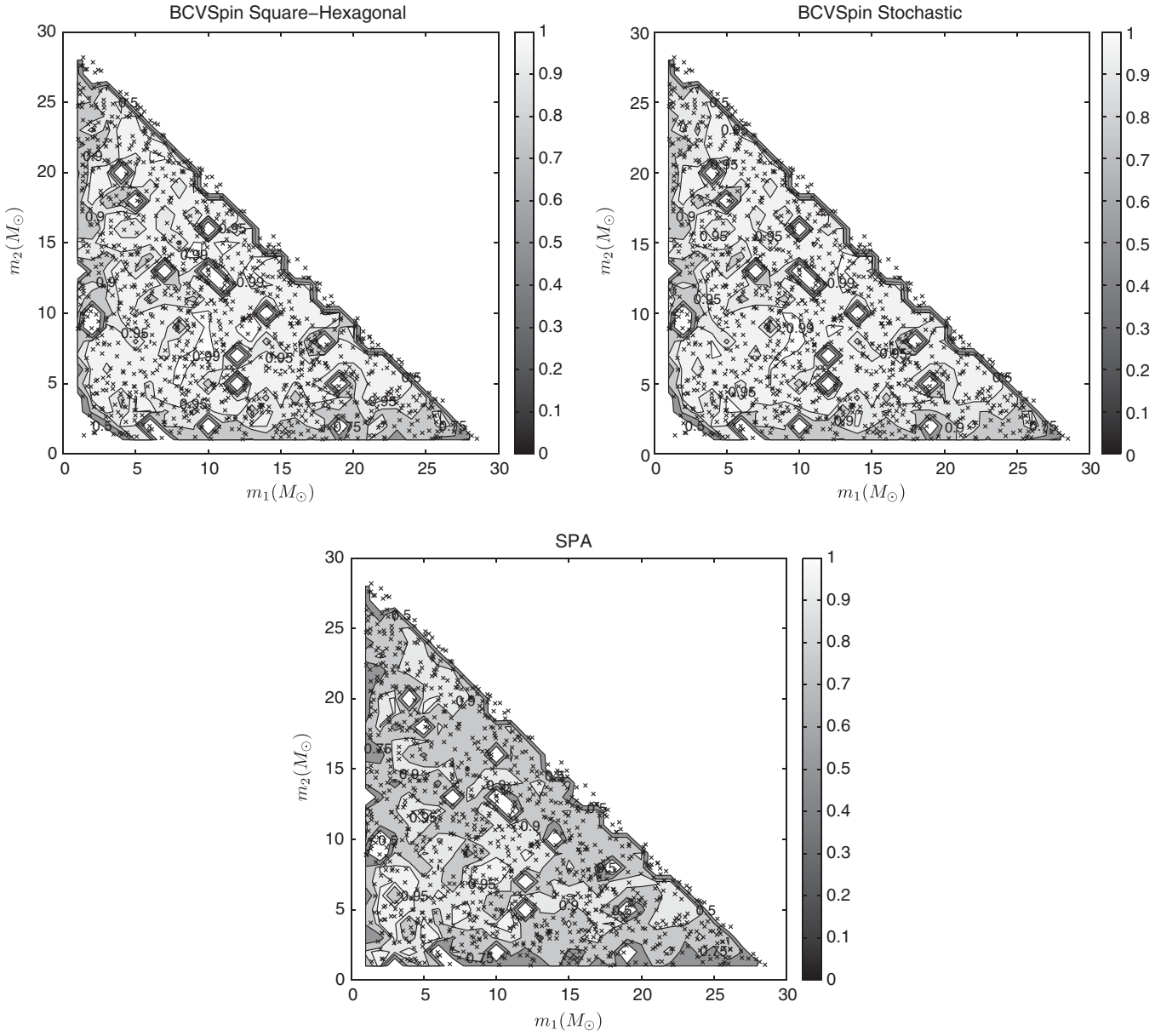

FIG. 1. Effective fitting factors of 1124 target waveforms with templates in a square-hexagonal BCV-spin bank (top left), a stochastic BCV-spin bank (top right), and an SPA bank using the Initial LIGO design PSD. The black crosses indicate the component masses for the target waveforms; spins have random orientations, and $0.7 \leq |\mathbf{S}_{1,2}/m_{1,2}^2| \leq 1$. The color coding gives the effective fitting factor of a target waveform over the template bank. There is no discernible difference between the performances of the square-hexagonal and stochastic BCV-spin banks, but both do notably better than SPA.

coincidence method, whereby two triggers are considered coincident if they occurred within a certain time from each other (say, 100 ms), and the associated templates have parameters that differ only within certain tolerances [73]. In the case of BCV spin, these were chosen as $\Delta\psi_0 = 40\,000\ \mathrm{Hz}^{5/3}$ and $\Delta\psi_3 = 600\ \mathrm{Hz}^{2/3}$, with no restrictions on differences in β [42].

More recently, a more sophisticated technique was developed which has the potential to dramatically reduce the false alarm rate [74]. In this method, the covariances between the signal parameters are used to define an error ellipsoid in parameter space around the triggers, and triggers in different detectors are considered coincident if their associated ellipsoids overlap. In the case of SPA banks, the size of the ellipsoids will depend strongly on the region of parameter space the triggers occur in. Generally, they will be smaller for triggers associated with smaller masses, as waveforms will then spend more time in the detector band and errors will be smaller. This leads to a dramatic reduction in the number of spurious coincident triggers. By

contrast, the box-coincidence method described above uses the same parameter windows anywhere in parameter space.

The ellipsoid coincidence method has been successfully implemented for SPA banks. The technique is well suited for banks where the templates are simplified versions of target waveforms, so that one can assume template waveforms to be reasonably close to physical signals. It would be possible in principle to implement such a method also for the (phenomenological) BCV-spin banks. However, in this case the metric $g_{ij}^{\rm eff}$ is basically independent of ψ_0 and ψ_3, the parameters that are most closely related to the masses. Hence, for a given value of β, the associated ellipsoids would not differ in size across (ψ_0, ψ_3) space, and only their orientations would differ with β. This way, no great improvements can be expected in terms of reducing the false alarm rate.

Table II shows the average number and variance of coincident triggers between the 4 km LIGO Hanford and Livingston detectors for time shifts within ~9 days of data from the fifth LIGO science run [1]. The SNR threshold for SPA is 5.5, while for BCV spin it is 8. With these thresholds, SPA and BCV-spin banks have approximately the same false alarm rates.

B. Efficiencies

We are now in a position to compare the efficiencies of SPA and BCV-spin banks. Given a large number of target waveforms injected in the data, the efficiency is the ratio of the number of found injections to the total number of injections made. For our purposes, an injection is considered found if it had an SNR above the chosen threshold with at least one template in the bank, within a certain time interval around the time when the injection was actually made. In the case of SPA, the width of this interval can be chosen to be 40 ms. BCV-spin templates, being phenomenological, turn out to have a larger timing inaccuracy, and an interval of 100 ms was found to be more appropriate. This had already been noticed in [42]; presumably the larger timing uncertainties of BCV spin are related to its unphysical phasing (essentially, missing PN terms) as it is predominantly the phasing which affects timing errors.

It is important that efficiencies be compared *for the same false alarm rate*. And indeed, as we have just seen, SPA and BCV spin have essentially the same background rates if the SNR thresholds are set at 5.5 and 8, respectively.

We made 1124 injections distributed logarithmically in distance between 1 and 50 Mpc, with component masses randomly chosen between $1M_\odot$ and $30M_\odot$, spin magnitudes $|\mathbf{S}_i|/m_i^2$, $i = 1, 2$ between 0.7 and 1, and arbitrary directions for the initial spin vectors. (As we mentioned before, astrophysical black holes are expected to have $|\mathbf{S}_i|/m_i^2 < 1$ [56], although in future studies it may be prudent to relax this restriction on injected signals to allow for possible violations of cosmic censorship.) The efficiency of SPA then came out to be 0.93, versus 0.89 for BCV spin. These results have been summarized in Appendix I of [45]; here we have provided a detailed account of how they were obtained. We refer to the latter paper for plots of efficiency against distance; see Table II for the distances at which the efficiencies are 50%, 75%, and 90%, both for SPA and stochastic BCV spin. As one would expect, the close-by missed injections tended to have parameters that would lead to significant precession of the orbital plane (i.e., asymmetric systems with significant misalignment of spins with orbital angular momentum).

We find that, despite the fact that BCV-spin banks have higher effective fitting factors with the target waveforms than SPA banks, in a more realistic data-analysis comparison the two waveform families have similar abilities to detect simulated signals. The detection statistic for BCV spin involves more degrees of freedom and the pipeline using BCV-spin waveforms is more sensitive to nonstationary noise transients in the data. Consequently, at the same false alarm rate the detection threshold of the BCV-spin bank is higher than the SPA bank, negating the effect of the improved effective fitting factor of the BCV-spin bank.[3] Searches for spinning binaries using the nonspinning bank therefore have approximately the same performance as even our improved BCV-spin bank. We emphasize that this is a statement regarding the detection problem. If a search with nonspinning banks were to lead to a serious detection candidate, then further investigations would have to involve much more realistic template waveforms, which would include spin.

TABLE II. Average number of triggers per time shifts ($\langle N\rangle$), and variances thereof ($\sigma = \langle N^2\rangle^{1/2}$), for SPA with $\mathcal{M} = 0.95$, and BCV spin with stochastic placement and $\mathcal{M} = 0.8$. Note that the 1-σ intervals overlap, so that the false alarm rates are comparable. Next to these we list distances at which the efficiencies are 50%, 75%, and 90%. See [45] for histograms of trigger numbers and efficiency plots.

Bank	$\langle N\rangle$	σ	$D_{50\%}$ (Mpc)	$D_{75\%}$ (Mpc)	$D_{90\%}$ (Mpc)
SPA	97.3	8.7	40.1	33.9	15.9
BCV spin	85.4	8.4	34.6	17.5	14.5

VII. CONCLUSIONS

Past searches for low-mass compact binary inspiral events in LIGO data (with the exception of [42]) have used waveforms which do not attempt to model the spin effects, despite the fact that astrophysical black holes may be spinning rapidly. In this paper we have constructed template banks using the BCV-spin waveform proposed in [40]. Though phenomenological, these waveforms seek to capture the spin-induced amplitude modulation one

[3]The problem had been anticipated in [40]; here we have quantified it using real data.

expects to see in a physical signal, and have high effective fitting factors with PN waveforms that include spin. We have improved on the search method of [42], in two ways: (i) we have constructed a bank using the metric outlined in Ref. [41], which is much better suited to the template family, and (ii) we have explored two new placement algorithms (square hexagonal and stochastic). We used spinning PN signals to study the effective fitting factors of three different banks: an SPA bank, a BCV-spin bank with square-hexagonal placement, and a BCV-spin bank with stochastic placement. We found that the two BCV-spin banks had a similar performance, but both did markedly better than SPA. However, search performance should be judged by detection efficiency at a given false alarm rate. The search pipeline for low-mass compact binaries ($2M_\odot \leq M \leq 35M_\odot$) in data from the fifth LIGO science run used a nonspinning SPA bank with an SNR threshold of 5.5. We have demonstrated that to achieve a comparable false alarm rate with the currently available search pipelines using BCV-spin templates requires an SNR threshold of 8 and with this higher threshold, the detection efficiency of BCV spin for spinning PN signals becomes similar to that of the nonspinning SPA pipeline. Our findings, presented at length here and summarized in Ref. [45], were used to guide the decision not to repeat the analysis of Ref. [42] with data from the fifth LIGO science run.

In conclusion, the detection performance of the BCV-spin pipeline is similar to that of the nonspinning SPA pipeline. We note, however, that our comparison is not entirely fair, because the SPA pipeline implements the metric-based coincidence algorithm of Ref. [74] which dramatically reduces the number of spurious coincident triggers. In principle, such a technique could also be applied for BCV spin, but since the metric has essentially no dependence on (ψ_0, ψ_3) and only a weak dependence on β it is unlikely that implementation of the metric-coincidence algorithm would improve the sensitivity of the BCV-spin pipeline. This justifies the use of nonspinning SPA pipelines rather than BCV-spin pipelines in LIGO searches. Nevertheless, to search for spinning signals with nonspinning banks is still suboptimal, and work is ongoing to improve the performance of searches for spinning signals using templates determined by physical (rather than phenomenological) parameters proposed in Refs. [67,75]. In the mean time, we recommend the continued use of nonspinning SPA banks in upcoming searches until more efficient template families designed to capture spin-modulated waveforms have been incorporated into a pipeline.

ACKNOWLEDGMENTS

We would like to thank the members of the LIGO Scientific Collaboration Compact Binary Coalescence group for many helpful discussions, and, in particular, Michele Vallisneri for a critical reading of the manuscript. C. V. D. B., T. C., I. H., G. J., and B. S. S. are supported by PPARC Grant No. PP/F001096/1. D. B. is supported by National Science Foundation Grant No. NSF-0847611. Hideyuki Tagoshi is supported by KAKENHI, No. 16540251 and No. 20540271. Hirotaka Takahashi is partially supported by the Uchida Energy Science Promotion Foundation, Sasagawa Scientific Research Grant and the JSPS Grant-in-Aid for Scientific Research No. 20540260.

[1] B. Abbott *et al.* (LIGO Scientific Collaboration), arXiv:0711.3041.
[2] F. Acernese *et al.* (Virgo Collaboration), AIP Conf. Proc. **794**, 307 (2005).
[3] B. Willke (LIGO Scientific Collaboration), Classical Quantum Gravity **24**, S389 (2007).
[4] B. Abbott *et al.* (unpublished).
[5] R. K. Kopparapu *et al.*, Astrophys. J. **675**, 1459 (2008).
[6] V. Kalogera *et al.*, Astrophys. J. **601**, L179 (2004); **614**, L137(E) (2004).
[7] R. O'Shaughnessy, C. Kim, V. Kalogera, and K. Belczynski, Astrophys. J. **672**, 479 (2008).
[8] R. O'Shaughnessy, C. Kim, T. Frakgos, V. Kalogera, and K. Belczynski, Astrophys. J. **633**, 1076 (2005).
[9] L. A. Wainstein and V. D. Zubakov, *Extraction of Signals from Noise* (Prentice-Hall, Englewood Cliffs, NJ, 1962).
[10] K. S. Thorne, in *Three Hundred Years of Gravitation*, edited by S. W. Hawking and W. Israel (Cambridge University Press, Cambridge, 1987), Chap. 9, pp. 330–458.
[11] L. Blanchet, T. Damour, and B. R. Iyer, Phys. Rev. D **51**, 5360 (1995).
[12] C. M. Will and A. G. Wiseman, Phys. Rev. D **54**, 4813 (1996).
[13] L. Blanchet, B. R. Iyer, C. M. Will, and A. G. Wiseman, Classical Quantum Gravity **13**, 575 (1996).
[14] L. Blanchet, Phys. Rev. D **54**, 1417 (1996).
[15] L. Blanchet, T. Damour, B. R. Iyer, C. M. Will, and A. G. Wiseman, Phys. Rev. Lett. **74**, 3515 (1995).
[16] L. Blanchet, G. Faye, B. R. Iyer, and B. Joguet, Phys. Rev. D **65**, 061501 (2002).
[17] L. Blanchet, T. Damour, G. Esposito-Farese, and B. R. Iyer, Phys. Rev. D **71**, 124004 (2005).
[18] L. Blanchet, T. Damour, G. Esposito-Farese, and B. R. Iyer, Phys. Rev. Lett. **93**, 091101 (2004).
[19] K. G. Arun, L. Blanchet, B. R. Iyer, and M. S. S. Qusailah, Classical Quantum Gravity **21**, 3771 (2004).
[20] L. Blanchet, G. Faye, B. R. Iyer, and S. Sinha, arXiv:0802.1249.

[21] L. E. Kidder, C. M. Will, and A. G. Wiseman, Phys. Rev. D **47**, R4183 (1993).
[22] L. E. Kidder, Phys. Rev. D **52**, 821 (1995).
[23] G. Faye, L. Blanchet, and A. Buonanno, Phys. Rev. D **74**, 104033 (2006).
[24] L. Blanchet, A. Buonanno, and G. Faye, Phys. Rev. D **74**, 104034 (2006).
[25] K. G. Arun, A. Buonanno, G. Faye, and E. Ochsner, Phys. Rev. D **79**, 104023 (2009).
[26] M. Hannam, S. Husa, U. Sperhake, B. Brügmann, and J. A. Gonzalez, Phys. Rev. D **77**, 044020 (2008).
[27] A. Buonanno, G. B. Cook, and F. Pretorius, Phys. Rev. D **75**, 124018 (2007).
[28] M. Boyle *et al.*, Phys. Rev. D **78**, 104020 (2008).
[29] A. Buonanno *et al.*, Phys. Rev. D **76**, 104049 (2007).
[30] A. Buonanno *et al.*, Phys. Rev. D **79**, 124028 (2009).
[31] B. J. Owen, Phys. Rev. D **53**, 6749 (1996).
[32] B. J. Owen and B. S. Sathyaprakash, Phys. Rev. D **60**, 022002 (1999).
[33] S. Babak, R. Balasubramanian, D. Churches, T. Cokelaer, and B. S. Sathyaprakash, Classical Quantum Gravity **23**, 5477 (2006).
[34] B. Allen, W. G. Anderson, P. R. Brady, D. A. Brown, and J. D. E. Creighton, arXiv:gr-qc/0509116.
[35] T. A. Apostolatos, C. Cutler, G. J. Sussman, and K. S. Thorne, Phys. Rev. D **49**, 6274 (1994).
[36] T. A. Apostolatos, Phys. Rev. D **52**, 605 (1995).
[37] T. A. Apostolatos, Phys. Rev. D **54**, 2438 (1996).
[38] V. Kalogera, Astrophys. J. **541**, 319 (2000).
[39] R. O'Shaughnessy, J. Kaplan, V. Kalogera, and K. Belczynski, Astrophys. J. **632**, 1035 (2005).
[40] A. Buonanno, Y. Chen, and M. Vallisneri, Phys. Rev. D **67**, 104025 (2003).
[41] A. Buonanno, Y. Chen, Y. Pan, H. Tagoshi, and M. Vallisneri, Phys. Rev. D **72**, 084027 (2005).
[42] B. Abbott *et al.* (LIGO Scientific Collaboration), Phys. Rev. D **78**, 042002 (2008).
[43] B. Abbott *et al.* (LIGO Scientific Collaboration), Phys. Rev. D **73**, 062001 (2006).
[44] B. Abbott *et al.* (LIGO Scientific Collaboration), Phys. Rev. D **77**, 062002 (2008).
[45] B. Abbott *et al.* (LIGO Scientific Collaboration), Phys. Rev. D **79**, 122001 (2009).
[46] T. Cokelaer, Phys. Rev. D **76**, 102004 (2007).
[47] B. Allen, I. Harry, and B. S. Sathyaprakash (unpublished).
[48] B. S. Sathyaprakash and S. V. Dhurandhar, Phys. Rev. D **44**, 3819 (1991).
[49] S. Droz, D. J. Knapp, E. Poisson, and B. J. Owen, Phys. Rev. D **59**, 124016 (1999).
[50] B. Abbott *et al.* (LIGO Scientific Collaboration), Phys. Rev. D **69**, 122001 (2004).
[51] B. Abbott *et al.* (LIGO Scientific Collaboration), Phys. Rev. D **72**, 082001 (2005).
[52] B. Abbott *et al.* (LIGO Scientific Collaboration), Phys. Rev. D **72**, 082002 (2005).
[53] B. Abbott *et al.* (LIGO Scientific Collaboration), Phys. Rev. D **73**, 102002 (2006).
[54] K. Belczynski, R. Taam, E. Rantsiou, and M. Van der Sluys, arXiv:astro-ph/0703131.
[55] G. B. Cook, S. L. Shapiro, and S. A. Teukolsky, Astrophys. J. **424**, 823 (1994).
[56] K. S. Thorne, Astrophys. J. **191**, 507 (1974).
[57] L. Blanchet, Living Rev. Relativity **5**, 3 (2002).
[58] T. Damour, B. R. Iyer, and B. S. Sathyaprakash, Phys. Rev. D **63**, 044023 (2001).
[59] L. Blanchet, B. R. Iyer, and B. Joguet, Phys. Rev. D **65**, 064005 (2002).
[60] T. Damour, P. Jaranowski, and G. Schaefer, Phys. Rev. D **62**, 084011 (2000).
[61] L. Blanchet, T. Damour, and G. Esposito-Farese, Phys. Rev. D **69**, 124007 (2004).
[62] L. Blanchet and B. R. Iyer, Phys. Rev. D **71**, 024004 (2005).
[63] L. Blanchet, T. Damour, and B. R. Iyer, Classical Quantum Gravity **22**, 155 (2005).
[64] H. Wahlquist, Gen. Relativ. Gravit. **19**, 1101 (1987).
[65] K. G. Arun, B. R. Iyer, B. S. Sathyaprakash, and P. A. Sundararajan, Phys. Rev. D **71**, 084008 (2005).
[66] L. Lindblom, B. J. Owen, and D. A. Brown, Phys. Rev. D **78**, 124020 (2008).
[67] Y. Pan, A. Buonanno, Y. Chen, and M. Vallisneri, Phys. Rev. D **69**, 104017 (2004).
[68] A. Buonanno, Y. Chen, and M. Vallisneri, Phys. Rev. D **67**, 024016 (2003).
[69] R. Prix, Classical Quantum Gravity **24**, S481 (2007).
[70] S. Babak, Classical Quantum Gravity **25**, 195011 (2008).
[71] C. Messenger, R. Prix, and M. A. Papa, Phys. Rev. D **79**, 104017 (2009).
[72] LSC Algorithm Library, http://www.lsc-group.phys.uwm.edu/lal.
[73] LIGO Scientific Collaboration, Technical Report LIGO-T070109-01, LIGO Project 2007, http://www.ligo.caltech.edu/docs/T/T070109-01.pdf.
[74] C. A. K. Robinson, B. S. Sathyaprakash, and A. S. Sengupta, Phys. Rev. D **78**, 062002 (2008).
[75] A. Buonanno, Y. Chen, Y. Pan, and M. Vallisneri, Phys. Rev. D **70**, 104003 (2004).